Nanoscale Advances

ROYAL SOCIETY OF CHEMISTRY

REVIEW

View Article Online
View Journal | View Issue

Cite this: *Nanoscale Adv.*, 2020, **2**, 2220

Recent advances in the template-confined synthesis of two-dimensional materials for aqueous energy storage devices

Zhengnan Tian,[a] Chaohui Wei[a] and Jingyu Sun *[ab]

Received 1st April 2020
Accepted 28th April 2020

DOI: 10.1039/d0na00257g

rsc.li/nanoscale-advances

The template-confined synthesis strategy is a simple and effective methodology to prepare two-dimensional nanomaterials. It has multiple advantages including green process, controllable morphology and adjustable crystal structure, and therefore, it is promising in the energy storage realm to synthesize high-performance electrode materials. In this review, we summarize the recent advances in the template-confined synthesis of two-dimensional nanostructures for aqueous energy storage applications. The material design is discussed in detail to accommodate target usage in aqueous supercapacitors and zinc metal batteries. The remaining challenges and future prospective are also covered.

1. Introduction

The growing demand for the miniaturization and multi-functionalization of electronic devices has stimulated the development of flexible and portable electrochemical energy storage (EES) devices.[1] Traditional alkali metal batteries, such as commercial lithium ion batteries, sodium ion batteries and potassium ion batteries, have been extensively attempted to aim for micro-EES devices. These systems normally adopt organic electrolytes to harvest favourable energy density and long durability. Nevertheless, their safety concerns due to the toxicity, flammability and corrosion of organic electrolytes pose a daunting threat.[2] In this respect, aqueous electrolyte-based EES devices such as aqueous supercapacitors,[3] aqueous zinc batteries (zinc ion batteries, zinc alkaline batteries and zinc air batteries) and aqueous alkali metal ion batteries have emerged as a research hotspot.[4–7] These aqueous systems are featured by high safety, excellent rate performance and ease-of-assembly, making it an ideal candidate for future portable EES.

The electrode material is an essential component in all EES devices; hence, strenuous efforts have been devoted to tailor its innovative structural and compositional design. In an aqueous electrolyte, the cation typically exhibits as hydrated forms such as $[Na(H_2O)_6]^+$, $[K(H_2O)_8]^+$, $[Mg(H_2O)_6]^{2+}$ and $[Al(H_2O)_6]^{3+}$, leading to a sizeable hydrated ionic radius in comparison with those in the organic electrolytes.[8,9] In line with this, exploring advanced materials with expanded layer spacings for rapid intercalation of ions is highly desirable, specifically for the

[a]College of Energy, Soochow Institute for Energy and Materials InnovationS (SIEMIS), Key Laboratory of Advanced Carbon Materials and Wearable Energy Technologies of Jiangsu Province, Soochow University, Suzhou 215006, P. R. China. E-mail: sunjy86@suda.edu.cn

[b]Beijing Graphene Institute, Beijing 100095, P. R. China

Zhengnan Tian received his BS degree from Soochow University in 2017. He is currently an MS candidate in College of Energy, Soochow Institute for Energy and Materials InnovationS (SIEMIS), Soochow University under the supervision of Prof. Jingyu Sun. His current research relates to aqueous energy storage devices and multi-field integrated systems.

Chaohui Wei received her bachelor's degree from Xi'an Jiaotong University in 2014 and her PhD from the University of Nottingham in 2019. She is currently a post-doctoral research fellow in College of Energy, Soochow University under the supervision of Prof. Jingyu Sun and Prof. Ruizhi Yang. Her current research interests focus on flexible and wearable energy storage devices, including Li–S and Zn–air batteries.

insertion reaction-based zinc ion batteries. With regard to aqueous supercapacitors, the key lies in the design of electrode components with either a large specific surface area to boost ion adsorption/desorption, or sufficient active sites to harness redox reactions. Accordingly, two-dimensional (2D) materials have come onto the stage, owing to their favourable properties toward electrochemical process. For instance, graphene and its derivatives (graphene oxide (GO) and reduced GO (rGO)) have served as the fundamental building blocks for various EES devices, rendering high electronic conductivity and special 2D morphology.[10] Other 2D materials, encompassing transition metal dichalcogenides (TMDs), metal–organic frameworks (MOFs), layered metal oxides (LMOs), layered double hydroxides (LDHs), MXene, *etc.*,[11] have also become promising candidates in emerging energy systems. Specifically, their unique physical and chemical features including the large interlayer distance, interconnected pores and sufficient active sites enable the effective promotion of electrochemical reaction kinetics.

To date, great attention has been garnered to the deployment of reliable synthesis strategies for target 2D materials with desired structures and properties. In general, there are two main synthetic streams for producing 2D materials: bottom-up and top-down routes. Bottom-up approach involves the liquid phase reaction (*e.g.*, organic ligand-assisted growth) and vapor phase reaction (*e.g.*, chemical vapor deposition). The top-down method mainly includes mechanical exfoliation of bulk materials in various media.[12] Of note, the bottom-up method is more widely adopted due to the versatile morphologies and the precisely controllable properties of final products. Indeed, there have been several review articles dealing with the introduction of different synthetic methods for 2D materials.[13] Amongst them, the template-confined strategy has been considered as a simple, effective and versatile bottom-up approach for synthesizing 2D nanostructures, which has advanced capability to well define the size, shape and configuration of target materials and holds a great implication for applications as compared with the other synthetic strategies. Nevertheless, recent reviews focusing on the template-confined growth strategy have rarely been reported.

Jingyu Sun earned his bachelor's degree (2008) from Zhejiang University and obtained his PhD (2013) from the University of Oxford. After two-year postdoc training with Prof. Zhongfan Liu at Peking University, he joined the University of Cambridge as a postdoctoral research fellow in 2015. Since March 2017 he became a full professor in College of Energy, Soochow University. His research interests center on CVD design of graphene materials and printing methodology for wearable energy systems.

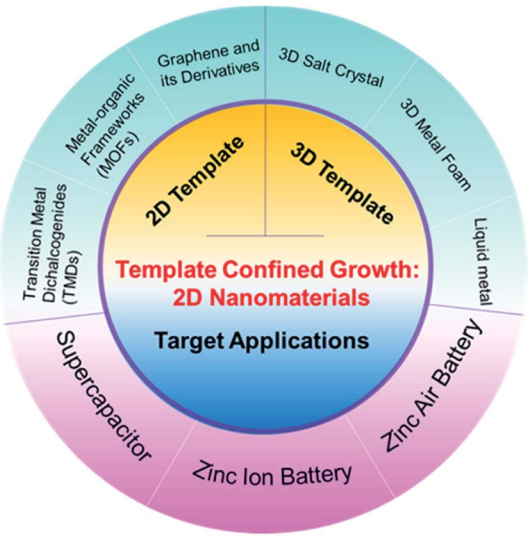

Scheme 1 Outline of the template-confined growth strategy of 2D materials and their related applications in aqueous energy storage devices.

Herein, we first summarize the synthetic methods of 2D materials *via* template-confined strategies, covering the employment of dimensional templates (Scheme 1). We then provide an overview of recent advances in the target applications such as aqueous supercapacitors, aqueous zinc ion batteries and zinc air batteries. Finally, we analyse the pros and cons of the synthetic methods and propose the future directions of the template-confined strategy for aqueous energy storage devices.

2. Synthesis strategy

The template-confined growth methodology is effective, feasible and universal amongst various synthetic strategies.[14] In general, the morphological templates induce liquid phase ions or gaseous molecules to grow along desired directions thanks to the distinct surface activities in different dimensions. Key parameters such as the adsorption energy barrier, catalytic activity and hydrophilic property could dictate the material growth. Usually, the growth along the *z*-direction is limited so as to form the 2D structure. Furthermore, the employed templates are stable to not participate in chemical reactions upon synthesis.[15] To fabricate the target materials, the template is required to have higher dimensions. Therefore, the dimension of such guiding agents for synthesizing 2D materials should be greater than or equal to two. In other words, templates possessing lower dimensions such as zero-dimensional quantum dots and one-dimensional nanowires are unlikely to form 2D productions. Accordingly, templates for the confined preparation of 2D materials are typically of 2D or three-dimensional (3D) forms, as demonstrated *vide infra*.

2.1. 2D templates

Various 2D materials themselves could act as excellent confined templates for the growth of designed 2D configurations, as the localized area restricts the growth along the *z*-direction. This

section summarizes the commonly used (graphene and its derivatives, TMDs, MOFs, LDHs, hydroxides and biomass metal oxides) and emerging (MXenes, stanenes and graphdiynes) 2D templates as confined growth agents.

2.1.1. Graphene and its derivatives. Graphene and its derivatives (GO and rGO), as the "star material", have been extensively exploited in the realm of energy storage due to their high conductivity, unique 2D morphology and good mechanical robustness.[16] In addition, their satisfactory tolerance to extreme environment and tailorable surface properties has by far ignited the interest in using them as hard templates to synthesize various 2D materials. In 2015, Sun *et al.* reported a synthetic strategy of GO/TiO_2 hybrid laminates using the monolayer GO as a universal template.[17] The hybrid exhibited excellent water desalination properties. Subsequently, Saito *et al.* proposed that the confined space between two GO layers were ideal for constructing various types of oxide layers. In this view, polycrystalline TiO_2, ZnO, Fe_2O_3 and amorphous SiO_2 were successfully deposited on the GO layers with a thickness of several nanometers.[18] Chen *et al.* also reported that graphene with various textures can be employed as versatile templates for preparing 2D metal oxide crystalline films with similar textures, including crumpled, wrinkled and hierarchical texture (Fig. 1). The intercalated metal ions were confined between van der Waals gaps of GO, followed by *in situ* conversion and annealing, wherein the ultrathin 2D metal oxide nanoplates (ZnO, Al_2O_3, Mn_2O_3 and CuO) were obtained.[19] The formation mechanism here is pertaining to two respects: (1) electrostatic attraction, where exists strong electrostatic adsorption between the intercalated metal ions and GO sheets (with a net negative potential: −50 mV) and (2) chemical complexation, in which carboxyl groups on the surface of GO have a large binding energy with metal ions, which is in favour of forming chemically specific ion-carboxylate complexation. Along with the fabrication of binary metal oxides, Abdelhamid *et al.* extended the same GO-templated method to produce ternary oxide nanosheets ($Ti_xNb_yO_z$, $Ni_xCo_yO_z$ and $Mn_xCo_yO_z$).[20] Moreover, complicated oxide species, such as $YBa_2Cu_3O_{7-\delta}$, can also be synthesized *via* the GO-templated strategy by Boston and his colleagues.[21]

It is worth noting that LDHs fabricated by such a GO-template method harvested large specific surface areas and enriched active sites.[22] In addition to the production of a wide variety of compounds, graphene and its derivatives can be employed as the space-confined templates to synthesize noble metals (*e.g.*, Au, Pt and Pd). Marangoni *et al.* developed a unique strategy of controllable growth of 2D gold with asymmetric nanostructures in aqueous media, using GO as a template (Fig. 2). Based on the microscopic investigations, gold nanoparticles underwent adsorption, nucleation and growth, readily forming a continuous 2D sheet on the GO template (with a ~5 nm thickness).[23]

Although graphene and its derivatives have been widely utilized as templates, stacking issues between graphene layers often affect the growth of 2D nanosheets. Moreover, aiming at removing the template, the additional calcination process might be detrimental to the surface properties of obtained products.

2.1.2. Transition metal dichalcogenides (TMDs). TMDs are typical 2D layered compounds with the chemical formula of MX_2, where M represents the transition metal (Fe, Mo, W, Mn, Re, V, *etc.*) and X denotes the chalcogen element (S, Se and Te). Similar to graphene, the van der Waals force between monolayers can offer suitable 2D confined spaces as the reaction platform to grow 2D materials. However, it is difficult to eliminate the TMD template after synthesis due to the non-volatility of metal elements upon annealing. In line with this, MoS_2 species has normally been employed as a hard template for forming 2D heterojunctions *in situ*.

Such 2D MoS_2 heterojunctions demonstrate widespread application potentials, *e.g.*, in the realm of electrocatalysis governed by interfacial defect engineering. Moreover, a MoS_2/metal/MoS_2 heterostructure has been employed as a high-frequency metal-base transistor. Moreover, several intriguing properties have been witnessed at the epitaxially grown metals on MoS_2. In 2013, Huang *et al.* reported an effective solution-phase growth, where Pd, Pt and Ag nanostructures could epitaxially grow on the MoS_2 (001) planes mainly with the (111) and (101) orientations.[24] Furthermore, a wide variety of thin

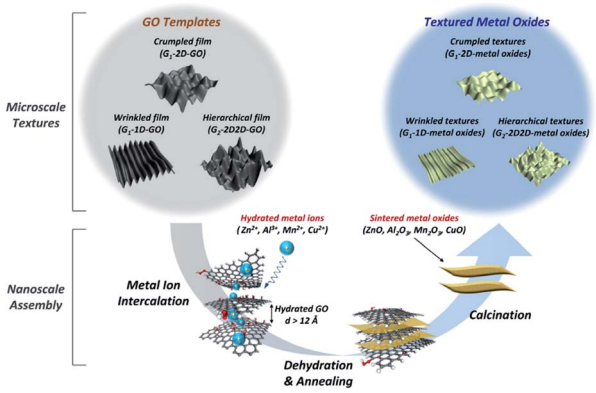

Fig. 1 Creation of hierarchical metal oxide architectures using textured GO as a versatile ion intercalation template. Reproduced with permission.[19] Copyright 2016, American Chemical Society.

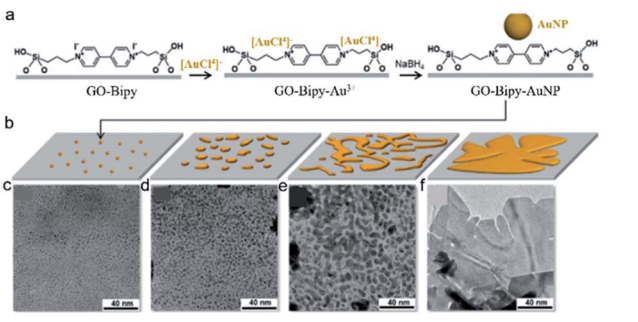

Fig. 2 (a) GO functionalization and the synthesis of gold nanoparticles (seeds). (b) Growing steps of the asymmetric 2D gold nanostructures. (c–f) Corresponding TEM images. Reproduced with permission.[23] Copyright 2018, Royal Society of Chemistry.

metal films including Al, Ag, Cu, Mn, Mo, Ni, Pd, Ru, Re, and Zn can be synthesized on monolayer MoS_2 due to the suitable lattice parameters.[25] To the best of our knowledge, several possible scenarios occur when MoS_2 and metal come into contact, such that new compounds could be formed, Mo or S lattices could be substituted by metal atoms, intercalation would be gained in between the MoS_2 layers, and/or the two materials could form an atomically abrupt interface. On the basis of this, metal/MoS_2 heterojunctions can be grown on MoS_2 throughout synergetic manipulation of thermodynamics and kinetics.

Different hybrid nanomaterials can be synthesized *via* choosing different metal precursors (K_2PtCl_4, K_2PdCl_4, $HAuCl_4$ or $AgNO_3$) and reduction routes (chemical reduction or photochemical reduction). Wu *et al.* constructed Mo_xC–graphene (Mo_xC–G) heterojunctions *in situ via* a MoS_2 atomic layer template.[26] Fig. 3a illustrates the growth procedures of Mo_xC–G. With the temperature increasing to 750 °C, the MoS_2 atomic layer was reduced to Mo, where the sulfur was volatilized. The metal Mo can subsequently act as the catalyst for graphene growth. Simultaneously, some Mo atoms were carburized to form Mo_xC supported on graphene. Viewing from the thermodynamics analysis, the direct reaction between bcc-Mo (hcp-Mo) structures and C_2H_4 tended to occur due to the energetic favourability compared with the starting reactants of MoS_2 and C_2H_4. In addition, the formation enthalpy of β-Mo_2C was much lower than those of other potentially formed compounds during the synthetic process of Mo_xC–G hybrids. Fig. 3b and c show the SEM images of Mo_xC–graphene composites, still maintaining the triangular template morphology. Fig. 3d and e verify the uniform distribution of Mo_xC nanoparticles on the surface of triangles. Nevertheless, it was noted that other TMDs have rarely been applied in the synthesis of 2D materials as the confined templates. In this regard, further efforts are required to develop simple and ubiquitous templating strategies to fabricate 2D materials and/or their heterojunctions.

In short, utilizing the TMDs as templates affords a feasible avenue to prepare 2D materials. However, in comparison with graphene templates, the removal of TMD templates remains a tough task.

2.1.3. Metal–organic frameworks (MOFs). 2D MOFs, generally formed by the coordination bonds between organic ligands and metal ion, have attracted growing attention because of the periodic structural unit.[27–30] For example, they have highly ordered pore structures, large specific surface areas, regulable metal components, and ample active sites.[31] The 2D layered structure, as a template, can provide the confined reaction space to grow certain 2D materials. More importantly, owing to the wide choices of metal elements and organic ligand molecules in MOFs, a variety of 2D nanosheets involving ultra-thin carbon, layered double hydroxide and metal oxide nanosheets can be easily prepared. The mainstream of MOF-derived 2D materials lies in the doped carbon nanosheets, encompassing the heteroatom dopants (N, P, B or S) and specific metal/metal oxide modifiers (Co, Ni, Fe, V, Mn, *etc.*). Kong *et al.* fabricated nitrogen-doped wrinkled carbon foils using a 2D Mn-MOF sacrificial template, where the MOF did not serve as a hard template but participated in the chemical reaction.[32] The main preparation process is depicted in Fig. 4a, mainly dealing with pyrolysis and etching. After annealing in ammonia, Na and Mn components/N-rich carbon foils (MNC-1) were derived. Subsequently, 2D porous nitrogen-doped carbon nanosheets (NC-1) can be formed upon acid treatment. Fig. 4b shows the TEM images of the bulk Mn-MOF (i), 2D Mn-MOF (ii), MNC-1 (iii) and NC-1 (iiii). Obviously, the final porous carbon nanosheets inherited the 2D structure of the original MOF template. During the gas phase reaction, gas molecules reacted, consumed, nucleated and grew in the confinement space on the surface of the MOF material, leading to the formation of 2D nanostructures. Indeed, the template method with the assistance of MOF materials is quite practicable. Notably, various 2D structures of metal oxides, phosphides, sulfides or selenides can be in target produced by changing the precursor salt and annealing atmosphere.[33–36]

Notwithstanding these advances, it should be noted that the elimination of the MOF template without any change is not an easy task. In addition, the inherently sophisticated pore

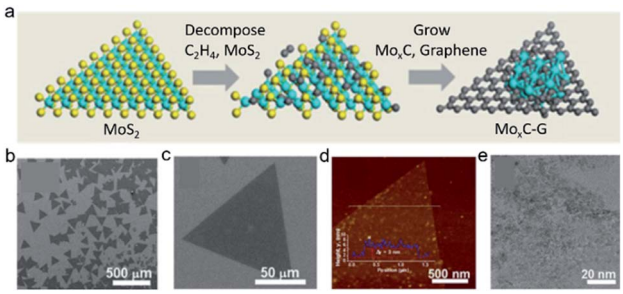

Fig. 3 Microscopic characterization of Mo_xC–G hybrids. (a) Illustration of the synthesis procedure of Mo_xC–G hybrids. The cyan, yellow, and gray spheres represent molybdenum, sulfur, and carbon atoms, respectively. (b and c) SEM images of Mo_xC–G. (d) AFM image of the Mo_xC–G flake on a SiO_2/Si substrate. The inset shows the height profile of the location as indicated by the solid white line. (e) TEM image of the Mo_xC–G hybrid. Reproduced with permission.[26] Copyright 2017, Wiley-VCH.

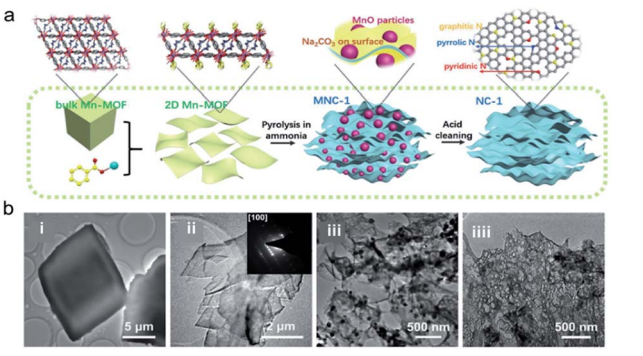

Fig. 4 (a) Schematic of the formation process of NC-1 from bulk Mn-MOF. (b) TEM images of the bulk Mn-MOF (i), 2D Mn-MOF (ii), MNC-1 (iii) and NC-1 (iiii). Reproduced with permission.[32] Copyright 2018, Wiley-VCH.

structure is more or less destroyed due to the elevated annealing temperature. Taking this into account, conductive MOF species are an effective material solution.

2.1.4. Other 2D templates. Other 2D templates, including, but not limited to, LDHs,[37] hydroxides[38] and 2D metal oxides,[39] have also been utilized to synthesize emerging 2D materials by the space-confined growth. A representative work by Wang *et al.* reported an innovative template route for synthesizing MoS_2 flakes in rhomboid shape with controllable layer numbers. The MoS_2 flakes were prepared by layer-by-layer sulfurization of MoO_2 microcrystals, wherein MoO_2 was employed as the reaction-confined platform and Mo source at the same time.[40] Inspired by this investigation, self-template strategies have been widely utilized in attaining a wide variety of 2D materials, such as NbS_2,[41] WS_2,[42] and SnS_2.[43]

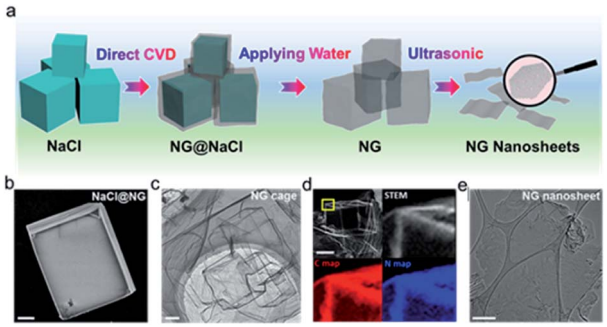

Fig. 5 (a) Schematic of the salt-templated CVD growth of NG nanosheets directly on the NaCl crystal. (b) SEM image of an individual NaCl@NG powder. (c) TEM image of the NG cage. (d) STEM image and elemental maps of the NG cage. (e) TEM image of the as-obtained NG nanosheet. Reproduced with permission.[44] Copyright 2019, American Chemical Society.

2.2. 3D templates

3D textured materials can also be employed as the guiding templates to synthesize 2D materials. Distinct from the 2D templating scenario, the confined growth can only occur at the surfaces of 3D templates. In turn, the 3D structures can be disintegrated throughout sonication to form 2D layers. In this section, typical 3D templates such as cubic salt crystals and metal foams are described.

2.2.1. 3D salt crystals. Salt, the most widely used template, is employed to synthesize materials of various types and scales, due to the low price, superior solubility in water and periodic unit cell. Along this line, Xiao *et al.* reported a generic salt-templated strategy for attaining 2D transition metal oxides, including hexagonal-MoO_3, MoO_2, MnO and hexagonal-WO_3.[15] The confined growth on the surface realized the matching of crystal lattices. Recently, Wei *et al.* have harnessed the CVD technology to synthesize nitrogen-doped graphene (NG) nanosheets by a NaCl template-assisted method.[44] The employment of plasma-enhanced CVD (PECVD) enabled the direct growth of NG nanosheets on a recrystallized salt crystal at relatively low temperatures (600–700 °C) in a controllable fashion, thereby creating a facile production process and lowering the production cost. Fig. 5a illustrates the typical fabrication. First, the NG nanosheet is conformally grown on NaCl cages with pyridine as both carbon and nitrogen sources. Then, the salt template is dissolved in deionized water by a simple washing procedure (the SEM and TEM images of NG hollow cages shown in Fig. 5b–d). Finally, 2D NG nanosheets can be directly formed through sonication. The growth on the surface is mainly attributed to different electric field intensities and catalytic activities of the gas molecules, such as the difference between the side face and the edge. Therefore, the fragile connection parts between the different side faces are easy to break up, resulting in the formation of uniform 2D nanosheets (Fig. 5e). In addition to metal oxides and graphenes,[45–47] 2D metal nitrides, sulfides, selenides and phosphides (*e.g.*, MoN, MoS_2, and MoP_2) can also be synthesized by virtue of salt-templated routes.[48–50]

For instance, in an attempt to synthesizing 2D metal phosphides, Li *et al.* developed a general salt-templating strategy. The fabrication process is shown in Fig. 6. $(NH_4)_2HPO_4$ is employed as a phosphorus source and mixed with metal nitrate precursors, which are then coated onto the surface of the salt template. The thus-obtained composites are annealed in a H_2/Ar atmosphere to generate various metal phosphides, such as Co_2P, MoP_2, $Ni_{12}P_5$ and WP_2.[51]

Another feasible strategy for obtaining 2D materials lies in using melted salt as the template. In contrast to the conventional mild condition with a processing temperature lower than 900 °C, this approach requires high-temperature annealing (over 900 °C). The droplets of molten salt act as a paradigm to induce separated flat structures to construct 2D nanoplates. In this regard, Zhu *et al.* used a melted $ZnCl_2$/KCl salt mixture as the porous template to grow vertically aligned graphitic carbon nanosheets and their metal carbide hybrids (WC, TaC and NbC).[52] In addition, ultrathin amorphous carbon nanosheets were synthesized by a molten-salt route in a scalable manner.[53]

2.2.2. 3D metal foams. 3D metal foams are often used as the template to fabricate 3D nanomaterials. For example, Ni foams can guide carbon species to form a porous hierarchical architecture. Subsequently, a 3D graphene foam can be prepared throughout a simple acid etching process.[54] Recently, Xing *et al.* have reported an effective synthesis route to attain high-crystalline g-C_3N_4 nanosheets by utilizing Ni foams as the confined template.[55] The scheme for the formation of 2D g-C_3N_4 nanosheets is shown in Fig. 7. The recrystallized process of dicyandiamide on the Ni surface occurs, followed by the pyrolysis

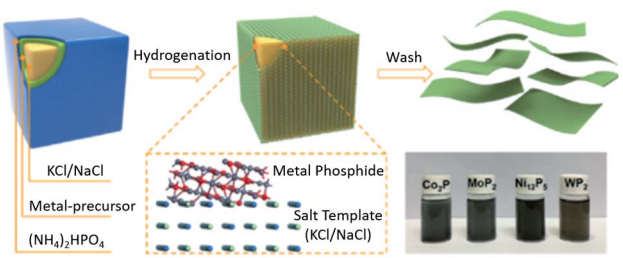

Fig. 6 Synthesis process of 2D metal phosphides. Reproduced with permission.[51] Copyright 2018, Royal Society of Chemistry.

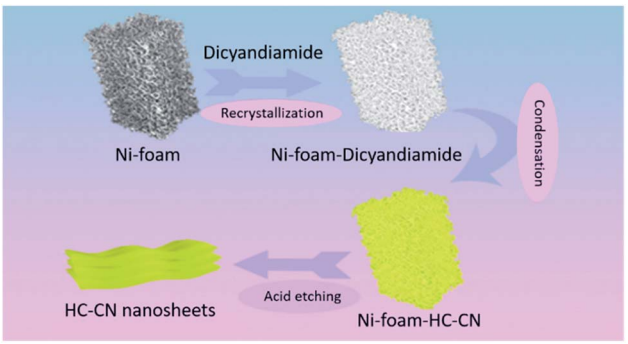

Fig. 7 Schematic of the formation of 2D g-C_3N_4 nanosheets. Reproduced with permission.[55] Copyright 2018, American Chemical Society.

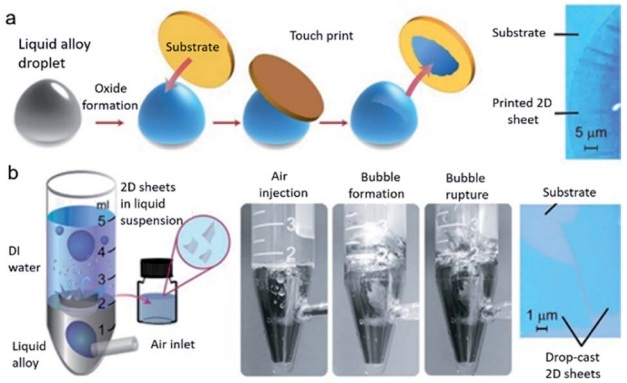

Fig. 8 (a) Schematic of the van der Waals exfoliation technique. The pristine liquid metal droplet is first exposed to an oxygen-containing environment. Touching the liquid metal with a suitable substrate allows transfer of the interfacial oxide layer. An optical image is shown at the right. (b) Schematic of the gas injection method (left), photographs of the bubble bursting through the liquid metal (center), and an optical image of the resulting sheets drop-casted onto a SiO_2/Si wafer (right). Reproduced with permission.[58] Copyright 2017, Science.

that would promote the surface-confined growth of C_3N_4, whilst the stacking of nanosheets are suppressed on a Ni foam. The 2D nanosheets were obtained *via* one-step acid etching. Taken together, the 3D metal foam is a favourable candidate due to its high catalytic activity (compared with non-metal 3D templates) and good mechanical stability to grow graphenes and/or other 2D materials. However, it is worth noting that metallic residuals and impurities could remain in target products due to any incomplete etching process of templates. Likewise, in comparison with the salt template route, the employment of acid etchants is normally environmentally unfriendly.

2.2.3. 3D liquid metal alloys. Owing to the unique structure of metallic cores and active surfaces, liquid metals and metal alloys show great potential for synthesizing 2D materials.[56] Liquid metals are featured by the surface effect of "self-limiting native-oxide skin", which was considered to be promising for preparing atomically thin materials.[57] In 2017, Zavabeti *et al.* reported the phenomenon that the self-limiting thin oxide layer occurred naturally in the gallium-based and other liquid metal alloys. Based on the observation, different atomically thin 2D materials such as HfO_2, Al_2O_3 and Gd_2O_3 were successfully achieved by manipulating different precursor elements in the alloys.[58] Two principal approaches for the isolation of the surface oxide are shown in Fig. 8. The former method is called van der Waals (vdW) exfoliation, where the metal oxide layers are easily exfoliated, owing to the weak combination between the metal core and the surface skin (Fig. 8a). The latter one is more scalable, utilizing the air bubble to remove the surface oxide skin (Fig. 8b). Following this innovative work, 2D GaS,[59] $GaPO_4$,[60] SnO,[61] AlOOH,[62] and GaN[63] can be in target prepared. Nevertheless, this strategy has certain limitations, where only 2D materials that are thermodynamically stable with liquid metals can be synthesized.

2.2.4. Other 3D templates. In addition, certain biomorphic architectures are feasible to function as templates benefiting from the 3D hierarchical configuration and enriched pore structures, such as diatomites.[64–66] It is an indirect method to grow 2D materials, compared with 2D templates. Nevertheless, it exhibits some distinct advantages including high yields and low by-product concentrations. Therefore, versatile 3D templates provide a new perspective for the synthesis of 2D materials.

3. Device applications

The application sectors of 2D materials cover a wide range of fields, including energy storage and conversion, sensing, and biomedicine. We herein pay special attention to the applications in aqueous energy storages. Owing to the distinct features, including high safety (compared with traditional organic electrolytes), high rate performance (high ion mobility within aqueous electrolytes), low pollution concern and operation feasibility, aqueous-based EES devices perfectly meet the current demands for flexible and wearable electronics.[4] However, the major challenge existing in this realm is the relatively unsatisfactory energy density, which stems from the undesirable electrode materials. In turn, acquisition of suitable cathode materials has become a bottleneck. In this regard, effective material design strategies, especially the abovementioned template-confined method, have been introduced to synthesize high-performance 2D materials to boost the energy density of aqueous-based EES systems. On the one hand, the ultrathin structure of the 2D materials provide a highly exposed surface area to facilitate electrolyte infiltration and ion adsorption, especially beneficial to the electric double-layer capacitive behaviour. Furthermore, various redox active species are easily decorated on the surface or layered space of 2D materials by a template-assisted method, resulting in heterojunction materials. The different components in heterostructure materials can synergistically enhance the charge storage in EES devices. On the other hand, the superior electron and ion conductivity of 2D materials is crucial for the electrode materials to promote electrochemical reactions and reduce electrochemical polarization, compared with other bulk materials. This section highlights the applications of template-confinement-derived 2D materials in supercapacitors and aqueous zinc metal batteries (zinc ion batteries and zinc air batteries). In a broader context, Table 1 summarizes the templates, obtained materials and versatile applications.

Table 1 Summary of the template-assisted materials and applications[a]

Templates	2D materials	Applications	Ref.
GO	$2GO/TiO_2$	Desalination	17
GO	$TiO_2/ZnO/Fe_2O_3/SiO_2$	LIB	18
GO	$ZnO/Al_2O_3/Mn_2O_3/CuO$	SC	19
GO	$Ti_xNb_yO_z/Ni_xCo_yO_z/Mn_xCo_yO_z$	LIB	20
GO	$YBa_2Cu_3O_{7-\delta}$	Superconducting	21
Graphene	LDH	SC	22
GO	Au	N/A	23
MoS_2	Pd/Pt/Ag	Electrocatalysis	24
MoS_2	Al/Ag/Cu/Mn/Mo/Ni/Pd/Ru/Re/Zn	N/A	25
MoS_2	Mo_xC-graphene	Electrocatalysis	26
rGO	MOF_S	LIB	30
Graphene	Conductive MOFs	SC	31
MOFs	N doped carbon	SIB	32
MOFs	$NiCo_2O_4$	SC	33
LDH	Au	Electrocatalysis	37
$Mg(OH)_2$	Graphene	SC	38
CuO	alpha-Fe_2O_3	Ferromagnetism	39
MoO_2	MoS_2	N/A	40
MoS_2	NbS_2	Memristors	41
Al_2O_3	WS_2	FET	42
NaCl	N doped graphene	SC	44
Na_2CO_3	Carbon	PIC	45
NaCl	Carbon	ZAB	46
NaCl	Carbon	LIC	47
NaCl	MoN	SC	48
ZIF-67	CoPO	Electrocatalysis	50
KCl/NaCl	$Co_2P/MoP_2/Ni_{12}P_5/WP_2$	Electrocatalysis	51
$ZnCl_2$/KCl	Graphitic carbon	LIB/electrocatalysis	52
KCl/$CaCl_2$	Amorphous carbon	LIB	53
Ni foam	g-C_3N_4	Electrocatalysis	55
Ga liquid	$HfO_2/Al_2O_3/Gd_2O_3$	N/A	58
Ga liquid	GaS	FET	59
Ga liquid	$GaPO_4$	N/A	60
Tin liquid	SnO	FET	61
Ga–Al liquid	AlOOH	Flux membranes	62
Ga liquid	GaN	FET	63
Diatomites	$VN/Mo_2N/WN$	SC	64
Diatomites	N-doped graphene	LSB	65
Polystyrene	MnO_2/N-doped carbon	SC	71
Pitch	g-C_3N_4	SC	72
MoS_2	Polypyrrole	SC	75
MXenes	Polypyrrole	SC	76
MOFs	MnO_x	ZIB	83
GO	MnO_2	ZIB	84
MOFs	$NiCo_2O_4$	ZIB	86
Ni foam	Co_3O_4	ZIB	87
Ni foam	Ni–Co LDH	ZIB	88
$Co(OH)_2$	MOFs	SC	90
MOF	MnO_2	SC	92
Ni foam	Ni_3S_2/Ni	ZIB	94
Ni foam	NiO/Ni	ZIB	95
GO	ZnO@RGO	ZIB	97
Graphene	Zn–Al LDH	ZIB	98
NaCl	Co_3O_4/Carbon	ZAB	112
MOFs	Co–N/C/MnO_2	ZAB	113
GO	Co_3O_4/Graphene	ZAB	114
$FeCl_3/SiO_2$	FeCo–N_x–carbon	ZAB	115
g-C_3N_4	N–P co-doped carbon	ZAB	115

[a] LIB: lithium ion battery; LIC: lithium ion capacitor; LSB: lithium-sulfur battery; SIB: sodium ion battery; PIC: potassium ion capacitor; SC: supercapacitor; ZIB: zinc ion battery; ZAB: zinc air battery; FET: field effect transistor.

3.1. Supercapacitors

Supercapacitors, featured by high power density (>10 000 W kg^{-1}) and impressive cycling stability (>10 000 cycles), manifest unique advantages in the large-scale grid systems. Nevertheless, the main shortcoming of such systems is the mediocre energy density (<10 W h kg^{-1}). The energy density of supercapacitors can be calculated according to the equation: $E = 1/2\ CV^2$. Therefore, it is of paramount significance to design suitable electrode materials with high capacitance for supercapacitors to realize advanced energy density.[3,67] As aforementioned, the template-confined method is beneficial for producing a variety of metal oxides,[68,69] nitrides,[70] and heteroatom-doped carbons,[71,72] which are promising candidates with pseudocapacitive features.

Typically, processing of 2D MXene flakes into hollow spheres and 3D architectures by a template method is reported by Zhao *et al.*[73] Inspired by this work, Yu *et al.* reported the 2D porous MXene ($Ti_3C_2T_x$) obtained by the melamine formaldehyde template, which were employed as the ink for 2D and 3D printing of supercapacitors.[74] The template-assisted strategy promoted the MXene to form an N-doped crumpled structure, showing great potentials for flexible and printable supercapacitors. The schematic of direct MXene-N ink printing is shown in Fig. 9. The N-doped porous structure can increase the surface area and conductivity to enhance ion diffusion. In terms of 2D screen printing, MXene-N micro-symmetrical supercapacitors delivered favourable areal capacitances (70.1/62.5 mF cm^{-2} at 10/100 mV s^{-1}). As for 3D printing, the MXene-N ink-based device also displayed high areal capacitances of 8.2, 5.2, and 3.4 F cm^{-2} for three-, two-, and one-layered electrodes respectively at a scan rate of 10 mV s^{-1}. The template-confined synthesis, when combined with printing technology, exhibits high potentials for supercapacitor applications.

It is worth mentioning that some conductive polymers can also be synthesized by the template confined method as electrode materials for supercapacitors. Tang and co-workers reported a feasible strategy to grow ultrathin polypyrrole films on MoS_2 monolayers, where the MoS_2 nanolayer was employed as both a self-confined template and an electrochemically active species.[75] The specific capacitance of MoS_2/PPy nanocomposites reached 700 F g^{-1} at a scan rate of 10 mV s^{-1} in the electrolyte of 1 M KCl. Significantly, the energy density of MoS_2/PPy can harvest 83.3 W h kg^{-1} at a power density of 3332 W kg^{-1}, outperforming other related studies in this field. Subsequently, Boota *et al.* utilized the layer spacing between titanium carbide as a reaction vessel to produce 2D polypyrrole. The Ti_3C_2Tx/PPy composite yielded the highest capacitance of 416 F g^{-1} at a scan rate of 5 mV s^{-1} with a durable long-term performance of 25 000 cycles.[76]

Taken together, the designed 2D nanomaterials *via* a template-confined strategy display unique advantages, such as controllable microstructure, large surface area and modulated elemental doping. Of note, in combination with emerging device fabrication technology (*e.g.*, printing), the thus-prepared 2D electrode materials would greatly contribute to increased energy density of supercapacitors.

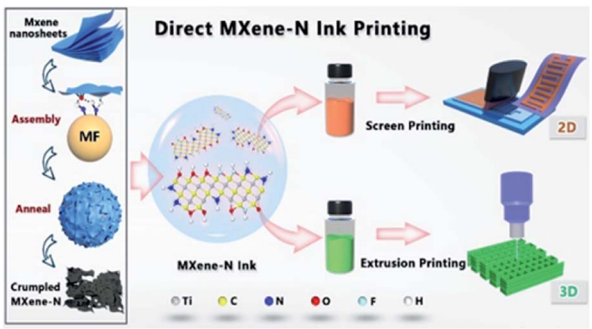

Fig. 9 Schematic of direct MXene-N ink printing. Left panel: synthesis of crumpled MXene-N. Right panel: versatile MXene-N inks designed for printing, namely, screen printing of the 2D pattern (top row) and extrusion printing of the 3D architecture (bottom row). Reproduced with permission.[74] Copyright 2019, Wiley-VCH.

3.2. Batteries

The aqueous batteries have already become a research hotspot, owing to their high safety and relatively high energy density. The aqueous battery system mainly includes alkali metal ion batteries (lithium, sodium and potassium ions) and multivalent ion batteries (zinc, magnesium, aluminium and calcium ions).[77] In this part, zinc metal batteries are chosen as a representative to discuss the significance of 2D materials synthesized by the templated strategy in the realm of aqueous batteries.[78]

3.2.1. Neutral zinc ion batteries. Neutral electrolyte-based zinc ion batteries store energy by the intercalation/deintercalation of zinc ions in the cathode but by the dissolution/deposition of zinc ions in the anode.[2] Consequently, the intercalated reaction mechanism requires fairly large layer spacings of electrode materials, rapid ion-solid phase diffusion rates and favourable structure stability. In this regard, 2D nanomaterials such as 2D van der Waals layered materials (MoS_2 and VS_2)[79,80] and layered metal oxides (V_2O_5 and MnO_2)[79,81–83] have become attractive due to the large interlayer spacings for Zn ion insertion. However, the major concern is raised from the electrode collapse upon cycling because of the fragile structure. Recently, Guo *et al.* have synthesized ultrathin δ-MnO_2 nanosheets by using GO as the template for aqueous Zn–MnO_2 batteries.[84] The as-prepared δ-MnO_2 nanosheets exhibited a favourable capacity of 133 mA h g^{-1} at a current density of 100 mA g^{-1} over 100 cycles. The ultrathin morphology facilitated the uniform current distribution and improved cycle stability. Another example by Ren *et al.* demonstrated the usage of polystyrene latex microspheres as templates to synthesize 2D porous MnO_2 nanosheets. The constructed Zn ion battery also showed a high specific capacity of 262.9 mA h g^{-1} at 300 mA g^{-1}.[85] Obviously, the template-confined growth strategy shows great advantages in the control of diversified hierarchical structures and accordingly enhances the electrochemical performance of neutral Zn ion batteries.

3.2.2. Alkaline zinc ion batteries. The reaction mechanism of alkaline electrolyte-based zinc ion batteries is somewhat different from that of the neutral systems. It lies in the reversible

redox reactions of hydroxyl groups on or near the surface, leading to the excellent rate performance and high energy density.[86] However, its development has been obstructed by the poor conductivity of cathode materials (Co_3O_4,[87] NiO, $Ni(OH)_2$, and Ni–Co-LDH[88,89]) and inferior stability of Zn plates in the alkaline media. As for the cathode material design, MOF architectures have been reported as sacrificial templates for the target synthesis of 2D carbons and metallic-based nanosheets. The metal phosphides and selenides, after a simple annealing process, can be easily obtained. Recently, Zeng *et al.* have synthesized the P–$NiCo_2O_{4-x}$ cathode material using MOF as the template, followed by annealing under $NaH_2PO_2 \cdot H_2O$.[86] The thus-fabricated P–$NiCo_2O_{4-x}$//Zn battery presented an impressive specific capacity of 361.3 mA h g^{-1} at a high current density of 3.0 A g^{-1} in an alkaline electrolyte. Briefly, the 2D MOF species, as a generic self-sacrificial template, offers great potential for the synthesis of desired cathode materials for alkaline Zn ion batteries. In particular, the adjustable metal source (Co MOFs,[90] Ni MOFs,[91] Mn MOFs,[92] and Fe MOFs[93]), the composite material (from the organic ligand) and modulated doped source (N, P, S, Se, and B doping) enable MOFs to act as versatile templates. The 2D materials from those MOFs can achieve increased conductivity and ample reactive sites, targeting the construction of high-performance alkaline Zn ion batteries. Certainly, in addition to the MOFs and its derivatives, the Ni foam could serve as a self-standing template to synthesize 2D nanosheets (Ni_3S_2/Ni,[94] NiO/Ni,[95] and Co_3S_4/Ni[96]) *in situ* without the post-removal of the foam. Apart from the cathode materials, the template-assisted synthesized 2D material is also employed as the anode in the alkaline zinc ion battery systems. For example, Sun *et al.* utilized GO as a template to synthesize 2D ZnO nanosheets, achieving a high capacity of 510 mA h g^{-1}.[97] Likewise, Yang *et al.* reported a Zn–Al LDHs/graphene composite by utilizing GO templates, harvesting a good cyclic stability (capacity retention: 94.9% after 800 cycles) as the anode material substituting the conventional ZnO/Zn anode.[98]

3.2.3. Zinc air batteries. Zinc air batteries gain merits in the high energy density and low safety concerns, which is considered as one of the most promising energy storage systems. Different from the reaction mechanisms mentioned above, it is based on surface catalytic reactions rather than solid phase ion intercalations or near-surface redox reactions.[99] Therefore, the key is to design effective cathode materials, which exhibit advanced catalytic activities for both oxygen evolution reactions (OERs) and oxygen reduction reactions (ORRs). The 2D nanosheets of doped carbons (N doped,[100] P doped,[101] S doped,[102] and B doped[103]) and/or metal compounds (Co_3O_4,[104] CoS,[105] CoN,[106] CoP,[107] Ni–FeN,[108] $CuCo_2S_4$,[109] Fe_2O_3,[110] and $NiCo_2O_4$ (ref. 111)), are widely probed as OER and ORR catalysts owing to the large surface area and enriched active sites. This, in turn, possesses huge implication in zinc air batteries. In this regard, the template-confined growth strategy is a suitable solution to synthesize cathode materials for Zn–air batteries. For instance, Ding and colleagues reported the preparation of 2D porous metal–based carbon nanosheets (Co–Co_3O_4/C) utilizing the melted NaCl salt as the template.[112] Upon high-temperature carbonization, the NaCl formed nanodroplets at 900 °C, where these nanodroplets penetrated into the interior of the carbon

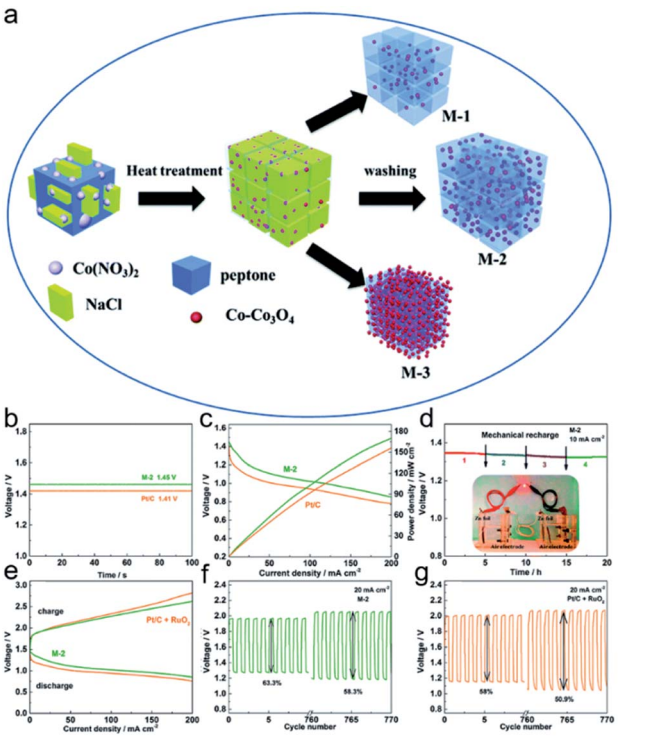

Fig. 10 (a) Synthesis route of Co–Co_3O_4/C samples. (b) Open circuit voltage of M-2 and Pt/C primary Zn–air batteries. (c) Polarization and power density curves. (d) Long-term galvanostatic discharge of the primary Zn–air battery. (e) Charge and discharge curves of the M-2 and Pt/C + RuO_2 cells. (f and g) Discharge and charge curves of current density: 20 mA cm^{-2}, electrolyte: 6 M KOH + 0.2 M $Zn(CH_3COO)_2$. Reproduced with permission.[112] Copyright 2019, Royal Society of Chemistry.

precursors and formed the 2D porous structure (shown in Fig. 10a). The final products were labelled as M-1 (0.2 g $Co(NO_3)_2 \cdot 6H_2O$), M-2 (0.4 g $Co(NO_3)_2 \cdot 6H_2O$) and M-3 (0.8 g $Co(NO_3)_2 \cdot 6H_2O$). From Fig. 10b–g, the as-derived Co–Co_3O_4/C nanosheets show favourable electrochemical performances, realizing high open circuit voltage, good rate performance and small polarization.

The salt template-assisted method aids to achieve thin 2D sheet structures, thereby enhancing the contact of electrolytes with electrodes and the rate of gas diffusion. Alongside the salt template, MOFs,[113] rGO,[114] silica,[115] g-C_3N_4 (ref. 116) have also been employed as templates to grow 2D nanosheets for Zn–air batteries. The template-confined approach tends to introduce various functional defects, providing a new perspective for the design of cathode materials for Zn–air batteries.

4. Conclusion and outlook

Continuously growing attention has been paid to 2D materials to date because of their fascinating structures and properties. A template-confined route has been investigated as a simple and universal strategy to synthesize 2D materials harnessing a wide suite of merits including abundant surface-active sites, large surface areas, enlarged layer spacings, controllable doping

amounts and tailored morphologies. In the foregoing sections, we summarized the recent advances in the realm of template-confined methods and the thus-derived 2D materials.

Nevertheless, there still exist several daunting challenges: (1) a relatively high cost aspect has to be maintained for the process of template production and subsequent template removal; (2) the sustainability of such a method deserves to be reconsidered, as the 2D template and 3D metal foam template are difficult to be recycled and reutilized; (3) certain templates are highly unlikely to be separated from the produced materials. For instance, it is a big task to remove the TMD or MOF templates. Interestingly, such "issues" can be useful in the *in situ* synthesis of heterojunctions and composites, which may lead to the realization of unique physical and chemical properties of materials.

Certainly, there is still a long way to utilize the template-assisted synthesized 2D materials to achieve higher energy density and rate performance for the aqueous EES devices. More importantly, how to take advantage of the template method and enlarge their role in energy storage systems is a question. In this respect, several solutions are proposed: (1) more attention could be paid to the employment of 2D materials in other components apart from electrodes, *i.e.*, functional separators, especially for aqueous Zn batteries; (2) there is large scope for research in aqueous hybrid capacitors, including Zn ion hybrid capacitors, K ion hybrid capacitors and Mg ion hybrid capacitors, where the 2D materials prepared *via* a template-confined route might serve as suitable electrodes. Indeed, smart utilization of various templates would not only alleviate the issues of material stacking and agglomeration during synthesis but also help creating innovative architectures with desired properties. It is anticipated that the template-confined growth strategies are versatile enough to produce high-quality 2D materials for aqueous energy storage applications in a practical manner.

Conflicts of interest

There are no conflicts to declare.

Acknowledgements

The authors acknowledge the support from the National Natural Science Foundation of China (51702225) and Natural Science Foundation of Jiangsu Province (BK20170336). The authors also acknowledge the support from Suzhou Key Laboratory for Advanced Carbon Materials and Wearable Energy Technologies, Suzhou, China.

References

1 S. Park, S. W. Heo, W. Lee, D. Inoue, Z. Jiang, K. Yu, H. Jinno, D. Hashizume, M. Sekino, T. Yokota, K. Fukuda, K. Tajima and T. Someya, Self-powered ultra-flexible electronics via nano-grating-patterned organic photovoltaics, *Nature*, 2018, **561**, 516–521.

2 X. Zeng, J. Hao, Z. Wang, J. Mao and Z. Guo, Recent progress and perspectives on aqueous Zn-based rechargeable batteries with mild aqueous electrolytes, *Energy Storage Materials*, 2019, **20**, 410–437.

3 Y. Shao, M. F. El-Kady, J. Sun, Y. Li, Q. Zhang, M. Zhu, H. Wang, B. Dunn and R. B. Kaner, Design and mechanisms of asymmetric supercapacitors, *Chem. Rev.*, 2018, **118**, 9233–9280.

4 C. Yang, J. Chen, X. Ji, T. P. Pollard, X. Lu, C. J. Sun, S. Hou, Q. Liu, C. Liu, T. Qing, Y. Wang, O. Borodin, Y. Ren, K. Xu and C. Wang, Aqueous Li-ion battery enabled by halogen conversion-intercalation chemistry in graphite, *Nature*, 2019, **569**, 245–250.

5 Y. Q. Li, H. Shi, S. B. Wang, Y. T. Zhou, Z. Wen, X. Y. Lang and Q. Jiang, Dual-phase nanostructuring of layered metal oxides for high-performance aqueous rechargeable potassium ion microbatteries, *Nat. Commun.*, 2019, **10**, 4292.

6 Q. Yang, S. Cui, Y. Ge, Z. Tang, Z. Liu, H. Li, N. Li, H. Zhang, J. Liang and C. Zhi, Porous single-crystal $NaTi_2(PO_4)_3$ via liquid transformation of TiO_2 nanosheets for flexible aqueous Na-ion capacitor, *Nano Energy*, 2018, **50**, 623–631.

7 J. Ming, J. Guo, C. Xia, W. Wang and H. N. Alshareef, Zinc-ion batteries: Materials, mechanisms, and applications, *Mater. Sci. Eng. R*, 2019, **135**, 58–84.

8 Z. Li, K. Xiang, W. Xing, W. C. Carter and Y.-M. Chiang, Reversible aluminum-ion intercalation in Prussian blue analogs and demonstration of a high-power aluminum-ion asymmetric capacitor, *Adv. Energy Mater.*, 2015, **5**, 1401410.

9 K. Li, Y. Shao, S. Liu, Q. Zhang, H. Wang, Y. Li and R. B. Kaner, Aluminum-ion-intercalation supercapacitors with ultrahigh areal capacitance and highly enhanced cycling stability: Power supply for flexible electrochromic devices, *Small*, 2017, **13**, 1700380.

10 R. Raccichini, A. Varzi, S. Passerini and B. Scrosati, The role of graphene for electrochemical energy storage, *Nat. Mater.*, 2015, **14**, 271–279.

11 Y. Dou, L. Zhang, X. Xu, Z. Sun, T. Liao and S. X. Dou, Atomically thin non-layered nanomaterials for energy storage and conversion, *Chem. Soc. Rev.*, 2017, **46**, 7338–7373.

12 Y. Chen, Z. Fan, Z. Zhang, W. Niu, C. Li, N. Yang, B. Chen and H. Zhang, Two-dimensional metal nanomaterials: Synthesis, properties, and applications, *Chem. Rev.*, 2018, **118**, 6409–6455.

13 R. Dong, T. Zhang and X. Feng, Interface-assisted synthesis of 2D materials: Trend and challenges, *Chem. Rev.*, 2018, **118**, 6189–6235.

14 Y. Liu, J. Goebl and Y. Yin, Templated synthesis of nanostructured materials, *Chem. Soc. Rev.*, 2013, **42**, 2610–2653.

15 X. Xiao, H. Song, S. Lin, Y. Zhou, X. Zhan, Z. Hu, Q. Zhang, J. Sun, B. Yang, T. Li, L. Jiao, J. Zhou, J. Tang and Y. Gogotsi, Scalable salt-templated synthesis of two-dimensional transition metal oxides, *Nat. Commun.*, 2016, **7**, 11296.

16 X. Zhang, L. Hou, A. Ciesielski and P. Samorì, 2D materials beyond graphene for high-performance energy storage applications, *Adv. Energy Mater.*, 2016, **6**, 1600671.
17 P. Sun, Q. Chen, X. Li, H. Liu, K. Wang, M. Zhong, J. Wei, D. Wu, R. Ma, T. Sasaki and H. Zhu, Highly efficient quasi-static water desalination using monolayer graphene oxide/titania hybrid laminates, *NPG Asia Mater.*, 2015, **7**, e162.
18 Y. Saito, X. Luo, C. Zhao, W. Pan, C. Chen, J. Gong, H. Matsumoto, J. Yao and H. Wu, Filling the gaps between graphene oxide: A general strategy toward nanolayered oxides, *Adv. Funct. Mater.*, 2015, **25**, 5683–5690.
19 P. Y. Chen, M. Liu, T. M. Valentin, Z. Wang, R. Spitz Steinberg, J. Sodhi, I. Y. Wong and R. H. Hurt, Hierarchical metal oxide topographies replicated from highly textured graphene oxide by intercalation templating, *ACS Nano*, 2016, **10**, 10869–10879.
20 A. A. AbdelHamid, J. H. Soh, Y. Yu and J. Y. Ying, Graphene oxide-templated synthesis of ternary oxide nanosheets for high-performance Li-ion battery anodes, *Nano Energy*, 2018, **44**, 399–410.
21 R. Boston, A. Bell, V. P. Ting, A. T. Rhead, T. Nakayama, C. F. J. Faul and S. R. Hall, Graphene oxide as a template for a complex functional oxide, *CrystEngComm*, 2015, **17**, 6094–6097.
22 D. Du, X. Wu, S. Li, Y. Zhang, W. Xing, L. Li, Q. Xue, P. Bai and Z. Yan, Remarkable supercapacitor performance of petal-like LDHs vertically grown on graphene/polypyrrole nanoflakes, *J. Mater. Chem. A*, 2017, **5**, 8964–8971.
23 V. S. Marangoni, L. D. Germano, C. C. C. Silva, E. A. de Souza and C. M. Maroneze, Engineering two-dimensional gold nanostructures using graphene oxide nanosheets as a template, *Nanoscale*, 2018, **10**, 13315–13319.
24 X. Huang, Z. Zeng, S. Bao, M. Wang, X. Qi, Z. Fan and H. Zhang, Solution-phase epitaxial growth of noble metal nanostructures on dispersible single-layer molybdenum disulfide nanosheets, *Nat. Commun.*, 2013, **4**, 1444.
25 A. C. Domask, K. A. Cooley, B. Kabius, M. Abraham and S. E. Mohney, Room temperature van der Waals epitaxy of metal thin films on molybdenum disulfide, *Cryst. Growth Des.*, 2018, **18**, 3494–3501.
26 J. Wu, L. Ma, A. Samanta, M. Liu, B. Li, Y. Yang, J. Yuan, J. Zhang, Y. Gong, J. Lou, R. Vajtai, B. Yakobson, A. K. Singh, C. S. Tiwary and P. M. Ajayan, Growth of molybdenum carbide-graphene hybrids from molybdenum disulfide atomic layer template, *Adv. Mater. Interfaces*, 2017, **4**, 1600866.
27 D. Feng, T. Lei, M. R. Lukatskaya, J. Park, Z. Huang, M. Lee, L. Shaw, S. Chen, A. A. Yakovenko, A. Kulkarni, J. Xiao, K. Fredrickson, J. B. Tok, X. Zou, Y. Cui and Z. Bao, Robust and conductive two-dimensional metal−organic frameworks with exceptionally high volumetric and areal capacitance, *Nat. Energy*, 2018, **3**, 30–36.
28 C. Liu, J. Wang, J. Wan, Y. Cheng, R. Huang, C. Zhang, W. Hu, G. Wei and C. Yu, Amorphous metal–organic framework dominated nanocomposites with both compositional and structural heterogeneity for oxygen evolution, *Angew. Chem., Int. Ed.*, 2020, **59**, 3630–3637.
29 Q. Jiang, P. Xiong, J. Liu, Z. Xie, Q. Wang, X. Yang, E. Hu, Y. Cao, J. Sun, Y. Xu and L. Chen, A redox-active 2D metal–organic framework for efficient lithium storage with extraordinary high capacity, *Angew. Chem., Int. Ed.*, 2020, **132**, 5311–5315.
30 C. Liu, X. Huang, J. Liu, J. Wang, Z. Chen, R. Luo, C. Wang, J. Li, L. Wang, J. Wan and C. Yu, A general approach to direct growth of oriented metal–organic framework nanosheets on reduced graphene oxides, *Adv. Sci.*, 2020, **7**, 1901480.
31 H. Wu, W. Zhang, S. Kandambeth, O. Shekhah, M. Eddaoudi and H. N. Alshareef, Conductive metal-organic frameworks selectively grown on laser-scribed graphene for electrochemical microsupercapacitors, *Adv. Energy Mater.*, 2019, **9**, 1900482.
32 L. Kong, J. Zhu, W. Shuang and X.-H. Bu, Nitrogen-doped wrinkled carbon foils derived from MOF nanosheets for superior sodium storage, *Adv. Energy Mater.*, 2018, **8**, 1801515.
33 C. Guan, X. Liu, W. Ren, X. Li, C. Cheng and J. Wang, Rational design of metal-organic framework derived hollow $NiCo_2O_4$ arrays for flexible supercapacitor and electrocatalysis, *Adv. Energy Mater.*, 2017, **7**, 1602391.
34 Y. Zhao, L. Hu, S. Zhao and L. Wu, Preparation of $MnCo_2O_4$@Ni(OH) core-shell flowers for asymmetric supercapacitor materials with ultrahigh specific capacitance, *Adv. Funct. Mater.*, 2016, **26**, 4085–4093.
35 H. Hu, Bu Y. Guan and X. W. Lou, Construction of complex CoS hollow structures with enhanced electrochemical properties for hybrid supercapacitors, *Chem*, 2016, **1**, 102–113.
36 L. Li, Y. Q. Zhang, X. Y. Liu, S. J. Shi, X. Y. Zhao, H. Zhang, X. Ge, G. F. Cai, C. D. Gu, X. L. Wang and J. P. Tu, One-dimension $MnCo_2O_4$ nanowire arrays for electrochemical energy storage, *Electrochim. Acta*, 2014, **116**, 467–474.
37 L. Wang, Y. Zhu, J. Q. Wang, F. Liu, J. Huang, X. Meng, J. M. Basset, Y. Han and F. S. Xiao, Two-dimensional gold nanostructures with high activity for selective oxidation of carbon-hydrogen bonds, *Nat. Commun.*, 2015, **6**, 6957.
38 J. Yan, Q. Wang, T. Wei, L. Jiang, M. Zhang, X. Jing and Z. Fan, Template-assisted low temperature synthesis of functionalized graphene for ultrahigh volumetric performance supercapacitors, *ACS Nano*, 2014, **8**, 4721–4729.
39 W. Cheng, J. He, T. Yao, Z. Sun, Y. Jiang, Q. Liu, S. Jiang, F. Hu, Z. Xie, B. He, W. Yan and S. Wei, Half-unit-cell alpha-Fe_2O_3 semiconductor nanosheets with intrinsic and robust ferromagnetism, *J. Am. Chem. Soc.*, 2014, **136**, 10393–10398.
40 X. Wang, H. Feng, Y. Wu and L. Jiao, Controlled synthesis of highly crystalline MoS_2 flakes by chemical vapor deposition, *J. Am. Chem. Soc.*, 2013, **135**, 5304–5307.
41 B. Wang, H. Luo, X. Wang, E. Wang, Y. Sun, Y.-C. Tsai, H. Zhu, P. Liu, K. Jiang and K. Liu, Bifunctional NbS_2-based asymmetric heterostructure for lateral and vertical electronic devices, *ACS Nano*, 2020, **14**, 175–184.

42 Y. Zhang, Y. Zhang, Q. Ji, J. Ju, H. Yuan, J. Shi, T. Gao, D. Ma, M. Liu and Y. J. A. n. Chen, Controlled growth of high-quality monolayer WS_2 layers on sapphire and imaging its grain boundary, *ACS Nano*, 2013, **7**, 8963–8971.

43 G. Su, V. G. Hadjiev, P. E. Loya, J. Zhang, S. Lei, S. Maharjan, P. Dong, P. M. Ajayan, J. Lou and H. J. N. l. Peng, Chemical vapor deposition of thin crystals of layered semiconductor SnS_2 for fast photodetection application, *Nano Lett.*, 2014, **15**, 506–513.

44 N. Wei, L. Yu, Z. Sun, Y. Song, M. Wang, Z. Tian, Y. Xia, J. Cai, Y. Y. Li, L. Zhao, Q. Li, M. H. Rummeli, J. Sun and Z. Liu, Scalable salt-templated synthesis of nitrogen-doped graphene nanosheets toward printable energy storage, *ACS Nano*, 2019, **13**, 7517–7526.

45 J. Chen, B. Yang, H. Hou, H. Li, L. Liu, L. Zhang and X. Yan, Disordered, large interlayer spacing, and oxygen-rich carbon nanosheets for potassium ion hybrid capacitor, *Adv. Energy Mater.*, 2019, **9**, 1803894.

46 Y. Wang, L. Tao, Z. Xiao, R. Chen, Z. Jiang and S. Wang, 3D carbon electrocatalysts in situ constructed by defect-rich nanosheets and polyhedrons from NaCl-sealed zeolitic imidazolate frameworks, *Adv. Funct. Mater.*, 2018, **28**, 1705356.

47 R. Shi, C. Han, H. Li, L. Xu, T. Zhang, J. Li, Z. Lin, C.-P. Wong, F. Kang and B. Li, NaCl-templated synthesis of hierarchical porous carbon with extremely large specific surface area and improved graphitization degree for high energy density lithium ion capacitors, *J. Mater. Chem. A*, 2018, **6**, 17057–17066.

48 X. Xiao, H. Yu, H. Jin, M. Wu, Y. Fang, J. Sun, Z. Hu, T. Li, J. Wu, L. Huang, Y. Gogotsi and J. Zhou, Salt-templated synthesis of 2D metallic MoN and other nitrides, *ACS Nano*, 2017, **11**, 2180–2186.

49 H. Wang, C. Ji, X. Zhang, Y. Sun, Y. Wang, Q. Pan and Q. Li, Synthesis of FeS nanoparticles embedded in MoS_2/C nanosheets as high-performance anode material for lithium-ion batteries, *Energy Technol*, 2019, **7**, 1801132.

50 G. Anandhababu, Y. Huang, D. Babu, M. Wu and Y. Wang, Oriented growth of ZIF-67 to derive 2D porous CoPO nanosheets for electrochemical-/photovoltage-driven overall water splitting, *Adv. Funct. Mater.*, 2018, **28**, 1706120.

51 T. Li, H. Jin, Z. Liang, L. Huang, Y. Lu, H. Yu, Z. Hu, J. Wu, B. Xia and G. Feng, Synthesis of single crystalline two-dimensional transition-metal phosphides via a salt-templating method, *Nanoscale*, 2018, **10**, 6844–6849.

52 J. Zhu, K. Sakaushi, G. Clavel, M. Shalom, M. Antonietti and T. P. Fellinger, A general salt-templating method to fabricate vertically aligned graphitic carbon nanosheets and their metal carbide hybrids for superior lithium ion batteries and water splitting, *J. Am. Chem. Soc.*, 2015, **137**, 5480–5485.

53 Y. Wang, W. Tian, L. Wang, H. Zhang, J. Liu, T. Peng, L. Pan, X. Wang and M. Wu, A tunable molten-salt route for scalable synthesis of ultrathin amorphous carbon nanosheets as high-performance anode materials for lithium-ion batteries, *ACS Appl. Mater. Interfaces*, 2018, **10**, 5577–5585.

54 K. Chen, L. Shi, Y. Zhang and Z. Liu, Scalable chemical-vapour-deposition growth of three-dimensional graphene materials towards energy-related applications, *Chem. Soc. Rev.*, 2018, **47**, 3018–3036.

55 W. Xing, W. Tu, Z. Han, Y. Hu, Q. Meng and G. Chen, Template-induced high-crystalline g-C_3N_4 nanosheets for enhanced photocatalytic H_2 evolution, *ACS Energy Lett*, 2018, **3**, 514–519.

56 X. Xiao, H. Wang, P. Urbankowski and Y. Gogotsi, Topochemical synthesis of 2D materials, *Chem. Soc. Rev.*, 2018, **47**, 8744–8765.

57 T. Daeneke, K. Khoshmanesh, N. Mahmood, I. de Castro, D. Esrafilzadeh, S. Barrow, M. Dickey and K. Kalantar-Zadeh, Liquid metals: fundamentals and applications in chemistry, *Chem. Soc. Rev.*, 2018, **47**, 4073–4111.

58 A. Zavabeti, J. Z. Ou, B. J. Carey, N. Syed, R. Orrell-Trigg, E. L. H. Mayes, C. Xu, O. Kavehei, A. P. O'Mullane and R. B. Kaner, A liquid metal reaction environment for the room-temperature synthesis of atomically thin metal oxides, *Science*, 2017, **358**, 332–335.

59 B. Carey, J. Ou, R. Clark, K. Berean, A. Zavabeti, A. Chesman, S. Russo, D. Lau, Z. Xu and Q. Bao, Wafer-scale two-dimensional semiconductors from printed oxide skin of liquid metals, *Nat. Commun.*, 2017, **8**, 14482.

60 N. Syed, A. Zavabeti, J. Ou, M. Mohiuddin, N. Pillai, B. Carey, B. Zhang, R. Datta, A. Jannat and F. Haque, Printing two-dimensional gallium phosphate out of liquid metal, *Nat. Commun.*, 2018, **9**, 3618.

61 T. Daeneke, P. Atkin, R. Orrell-Trigg, A. Zavabeti, T. Ahmed, S. Walia, M. Liu, Y. Tachibana, M. Javaid and A. Greentree, Wafer-scale synthesis of semiconducting SnO monolayers from interfacial oxide layers of metallic liquid tin, *ACS Nano*, 2017, **11**, 10974–10983.

62 A. Zavabeti, B. Zhang, I. Castro, J. Ou, B. Carey, M. Mohiuddin, R. Datta, C. Xu, A. Mouritz and C. McConville, Green synthesis of low-dimensional aluminum oxide hydroxide and oxide using liquid metal reaction media: Ultrahigh flux membranes, *Adv. Funct. Mater.*, 2018, **28**, 1804057.

63 Y. Chen, K. Liu, J. Liu, T. Lv, B. Wei, T. Zhang, M. Zeng, Z. Wang and L. Fu, Growth of 2D GaN single crystals on liquid metals, *J. Am. Chem. Soc.*, 2018, **140**, 16392–16395.

64 Y. Yi, L. Yu, Z. Tian, Y. Song, Y. Shao, L. Gao, J. Sun and Z. Liu, Biotemplated synthesis of transition metal nitride architectures for flexible printed circuits and wearable energy storages, *Adv. Funct. Mater.*, 2018, **28**, 1805510.

65 Q. Li, Y. Song, R. Xu, L. Zhang, J. Gao, Z. Xia, Z. Tian, N. Wei, M. H. Rummeli, X. Zou, J. Sun and Z. Liu, Biotemplating growth of nepenthes-like N-doped graphene as a bifunctional polysulfide scavenger for Li–S batteries, *ACS Nano*, 2018, **12**, 10240–10250.

66 T. Guo, Y. Song, Z. Sun, Y. Wu, Y. Xia, Y. Li, J. Sun, K. Jiang, S. Dou and J. Sun, Bio-templated formation of defect-abundant VS_2 as a bifunctional material toward high-performance hydrogen evolution reactions and lithium–sulfur batteries, *J. Energy Chem.*, 2020, **42**, 34–42.

67 Z. Tian, X. Tong, G. Sheng, Y. Shao, L. Yu, V. Tung, J. Sun, R. B. Kaner and Z. Liu, Printable magnesium ion quasi-solid-state asymmetric supercapacitors for flexible solar-charging integrated units, *Nat. Commun.*, 2019, **10**, 4913.

68 P. Liu, Y. Zhu, X. Gao, Y. Huang, Y. Wang, S. Qin and Y. Zhang, Rational construction of bowl-like MnO_2 nanosheets with excellent electrochemical performance for supercapacitor electrodes, *Chem. Eng. J.*, 2018, **350**, 79–88.

69 T. Kou, B. Yao, T. Liu and Y. Li, Recent advances in chemical methods for activating carbon and metal oxide-based electrodes for supercapacitors, *J. Mater. Chem. A*, 2017, **5**, 17151–17173.

70 Y. Zhong, X. Xia, F. Shi, J. Zhan, J. Tu and H. Fan, Transition metal carbides and nitrides in energy storage and conversion, *Adv. Sci.*, 2016, **3**, 1500286.

71 H. Liu, D. Zhai, M. Wang, J. Liu, X. Chen and Z. Zhang, Urea-modified phenol-formaldehyde resins for the template-assisted synthesis of nitrogen-doped carbon nanosheets as electrode material for supercapacitors, *ChemElectroChem*, 2019, **6**, 885–891.

72 D. Wang, Y. Wang, Y. Chen, W. Liu, H. Wang, P. Zhao, Y. Li, J. Zhang, Y. Dong, S. Hu and J. Yang, Coal tar pitch derived N-doped porous carbon nanosheets by the in-situ formed g-C_3N_4 as a template for supercapacitor electrodes, *Electrochim. Acta*, 2018, **283**, 132–140.

73 M. Zhao, X. Xie, C. Ren, T. Makaryan, B. Anasori, G. Wang and Y. Gogotsi, Hollow MXene spheres and 3D macroporous MXene frameworks for Na-ion storage, *Adv. Mater.*, 2017, **29**, 1702410.

74 L. Yu, Z. Fan, Y. Shao, Z. Tian, J. Sun and Z. Liu, Versatile N-doped MXene ink for printed electrochemical energy storage application, *Adv. Energy Mater.*, 2019, **9**, 1901839.

75 H. Tang, J. Wang, H. Yin, H. Zhao, D. Wang and Z. Tang, Growth of polypyrrole ultrathin films on MoS_2 monolayers as high-performance supercapacitor electrodes, *Adv. Mater.*, 2015, **27**, 1117–1123.

76 M. Boota, B. Anasori, C. Voigt, M. Zhao, M. Barsoum and Y. Gogotsi, Pseudocapacitive electrodes produced by oxidant-free polymerization of pyrrole between the layers of 2D titanium carbide (MXene), *Adv. Mater.*, 2016, **28**, 1517–1522.

77 L. Dong, W. Yang, W. Yang, Y. Li, W. Wu and G. Wang, Multivalent metal ion hybrid capacitors: a review with a focus on zinc-ion hybrid capacitors, *J. Mater. Chem. A*, 2019, **7**, 13810–13832.

78 M. Song, H. Tan, D. Chao and H. Fan, Recent advances in Zn-ion batteries, *Adv. Funct. Mater.*, 2018, **28**, 1802564.

79 H. Li, Q. Yang, F. Mo, G. Liang, Z. Liu, Z. Tang, L. Ma, J. Liu, Z. Shi and C. Zhi, MoS_2 nanosheets with expanded interlayer spacing for rechargeable aqueous Zn-ion batteries, *Energy Storage Materials*, 2019, **19**, 94–101.

80 P. He, M. Yan, G. Zhang, R. Sun, L. Chen, Q. An and L. Mai, Layered VS_2 nanosheet-based aqueous Zn ion battery cathode, *Adv. Energy Mater.*, 2017, **7**, 1601920.

81 D. Chao, W. Zhou, C. Ye, Q. Zhang, Y. Chen, L. Gu, K. Davey and S. Qiao, An electrolytic Zn-MnO_2 battery for high-voltage and scalable energy storage, *Angew. Chem., Int. Ed.*, 2019, **58**, 7823–7828.

82 M. Yan, P. He, Y. Chen, S. Wang, Q. Wei, K. Zhao, X. Xu, Q. An, Y. Shuang, Y. Shao, K. Mueller, L. Mai, J. Liu and J. Yang, Water-lubricated intercalation in $V_2O_5.nH_2O$ for high-capacity and high-rate aqueous rechargeable zinc batteries, *Adv. Mater.*, 2018, **30**, 1703725.

83 Y. Fu, Q. Wei, G. Zhang, X. Wang, J. Zhang, Y. Hu, D. Wang, L. Zuin, T. Zhou, Y. Wu and S. Sun, High-performance reversible aqueous Zn-ion battery based on porous M_nO_x nanorods coated by MOF-derived N-doped carbon, *Adv. Energy Mater.*, 2018, **8**, 1801445.

84 C. Guo, H. Liu, J. Li, Z. Hou, J. Liang, J. Zhou, Y. Zhu and Y. Qian, Ultrathin δ-MnO_2 nanosheets as cathode for aqueous rechargeable zinc ion battery, *Electrochim. Acta*, 2019, **304**, 370–377.

85 H. Ren, J. Zhao, L. Yang, Q. Liang, S. Madhavi and Q. Yan, Inverse opal manganese dioxide constructed by few-layered ultrathin nanosheets as high-performance cathodes for aqueous zinc-ion batteries, *Nano Res.*, 2019, **12**, 1347–1353.

86 Y. Zeng, Z. Lai, Y. Han, H. Zhang, S. Xie and X. Lu, Oxygen-vacancy and surface modulation of ultrathin nickel cobaltite nanosheets as a high-energy cathode for advanced Zn-ion batteries, *Adv. Mater.*, 2018, **30**, 1802396.

87 X. Wang, F. Wang, L. Wang, M. Li, Y. Wang, B. Chen, Y. Zhu, L. Fu, L. Zha, L. Zhang, Y. Wu and W. Huang, An aqueous rechargeable Zn//Co_3O_4 battery with high energy density and good cycling behavior, *Adv. Mater.*, 2016, **28**, 4904–4911.

88 H. Chen, Z. Shen, Z. Pan, Z. Kou, X. Liu, H. Zhang, Q. Gu, C. Guan and J. Wang, Hierarchical micro-nano sheet arrays of nickel-cobalt double hydroxides for high-rate Ni-Zn batteries, *Adv. Sci.*, 2019, **6**, 1802002.

89 Y. Zeng, Y. Meng, Z. Lai, X. Zhang, M. Yu, P. Fang, M. Wu, Y. Tong and X. Lu, An ultrastable and high-performance flexible fiber-shaped Ni-Zn battery based on a Ni-NiO heterostructured nanosheet cathode, *Adv. Mater.*, 2017, **29**, 1702698.

90 T. Deng, Y. Lu, W. Zhang, M. Sui, X. Shi, D. Wang and W. Zheng, Inverted design for high-performance supercapacitor via $Co(OH)_2$-derived highly oriented MOF electrodes, *Adv. Energy Mater.*, 2018, **8**, 1702294.

91 Q. Cheng, K. Tao, X. Han, Y. Yang, Z. Yang, Q. Ma and L. Han, Ultrathin Ni-MOF nanosheet arrays grown on polyaniline decorated Ni foam as an advanced electrode for asymmetric supercapacitors with high energy density, *Dalton Trans.*, 2019, **48**, 4119–4123.

92 K. Zhao, Z. Xu, Z. He, G. Ye, Q. Gan, Z. Zhou and S. Liu, Vertically aligned MnO_2 nanosheets coupled with carbon nanosheets derived from Mn-MOF nanosheets for supercapacitor electrodes, *J. Mater. Sci.*, 2018, **53**, 13111–13125.

93 X. Zhang, Q. Liu, X. Shi, A. Asiri and X. Sun, An Fe-MOF nanosheet array with superior activity towards the alkaline oxygen evolution reaction, *Inorg. Chem. Front.*, 2018, **5**, 1405–1408.

94 Z. Huang, X. Li, Q. Yang, L. Ma, F. Mo, G. Liang, D. Wang, Z. Liu, H. Li and C. Zhi, Ni_3S_2/Ni nanosheet arrays for high-performance flexible zinc hybrid batteries with evident two-stage charge and discharge processes, *J. Mater. Chem. A*, 2019, **7**, 18915.

95 Q. Chen, J. Li, C. Liao, G. Hu, Y. Fu, O. Asare, S. Shi, Z. Liu, L. Zhou and L. Mai, Ni foam supported NiO nanosheets as high-performance free-standing electrodes for hybrid supercapacitors and Ni–Zn batteries, *J. Mater. Chem. A*, 2018, **6**, 19488.

96 Si. Zhang, B. Yin, Y. Luo, L. Shen, B. Tang, Z. Kou, X. Liu, D. Lim, D. Gu, Z. Wang and H. Gong, Fabrication and theoretical investigation of cobaltosic sulfide nanosheets for flexible aqueous Zn/Co batteries, *Nano Energy*, 2020, **68**, 104314.

97 L. Sun, Z. Yi, J. Lin, F. Liang, Y. Wu, Z. Cao and L. Wang, Fast and energy efficient synthesis of ZnO@RGO and its application in Ni−Zn secondary battery, *J. Phys. Chem. C*, 2016, **120**, 12337–12343.

98 H. Yang, Z. Yang, X. Wen and L. Liu, The in-situ growth of zinc-aluminium layered double hydroxides on graphene and its application as anode active materials for Zn-Ni secondary battery, *Electrochim. Acta*, 2017, **252**, 507–515.

99 H. Wang, C. Tang and Q. Zhang, A review of precious-metal-free bifunctional oxygen electrocatalysts: Rational design and applications in Zn−air batteries, *Adv. Funct. Mater.*, 2018, **28**, 1803329.

100 L. Wang, C. Yang, S. Dou, S. Wang, J. Zhang, X. Gao, J. Ma and Y. Yu, Nitrogen-doped hierarchically porous carbon networks: synthesis and applications in lithium-ion battery, sodium-ion battery and zinc-air battery, *Electrochim. Acta*, 2016, **219**, 592–603.

101 W. Lei, O. Deng, G. Li, Z. Cano, X. Wang, D. Luo, Y. Liu, D. Wang and Z. Chen, Two-dimensional phosphorus-doped carbon nanosheets with tunable porosity for oxygen reactions in zinc-air batteries, *ACS Catal.*, 2018, **8**, 2464–2472.

102 Y. Su, Z. Yao, F. Zhang, H. Wang, Z. Mics, E. Cánovas, M. Bonn, X. Zhuang and X. Feng, Sulfur-enriched conjugated polymer nanosheet derived sulfur and nitrogen co-doped porous carbon nanosheets as electrocatalysts for oxygen reduction reaction and zinc-air battery, *Adv. Funct. Mater.*, 2016, **26**, 5893–5902.

103 Y. Guo, P. Yuan, J. Zhang, Y. Hu, I. Amiinu, X. Wang, J. Zhou, H. Xia, Z. Song, Q. Xu and S. Mu, Carbon nanosheets containing discrete Co-N_x-B_y-C active sites for efficient oxygen electrocatalysis and rechargeable Zn–Air Batteries, *ACS Nano*, 2018, **12**, 1894–1901.

104 L. Xu, Q. Jiang, Z. Xiao, X. Li, J. Huo, S. Wang and L. Dai, Plasma-engraved Co_3O_4 nanosheets with oxygen vacancies and high surface area for the oxygen evolution reaction, *Angew. Chem., Int. Ed.*, 2016, **55**, 5277–5281.

105 J. Yin, Y. Li, F. Lv, M. Lu, K. Sun, W. Wang, L. Wang, F. Cheng, Y. Li, P. Xi and S. Guo, Oxygen vacancies dominated NiS_2/CoS_2 interface porous nanowires for portable Zn–Air batteries driven water splitting devices, *Adv. Mater.*, 2017, **29**, 1704681.

106 Q. Xu, H. Jiang, Y. Li, D. Liang, Y. Hu and C. Li, In-situ enriching active sites on co-doped Fe-Co_4N@N-C nanosheet array as air cathode for flexible rechargeable Zn-air batteries, *Appl. Catal., B*, 2019, **256**, 117893.

107 X. Qin, Z. Wang, J. Han, Y. Luo, F. Xie, G. Cui, X. Guo and X. Sun, Fe-doped CoP nanosheet arrays: an efficient bifunctional catalyst for zinc–air batteries, *Chem. Commun.*, 2018, **54**, 7693–7696.

108 Y. Fan, S. Ida, A. Staykov, T. Akbay, H. Hagiwara, J. Matsuda, K. Kaneko and T. Ishihara, Ni-Fe nitride nanoplates on nitrogen-doped graphene as a synergistic catalyst for reversible oxygen evolution reaction and rechargeable Zn-Air battery, *Small*, 2017, **13**, 1700099.

109 Y. Li, J. Yin, L. An, M. Lu, K. Sun, Y. Zhao, F. Cheng and P. Xi, Metallic $CuCo_2S_4$ nanosheets of atomic thickness as efficient bifunctional electrocatalysts for portable, flexible Zn-air batteries, *Nanoscale*, 2018, **10**, 6581–6588.

110 Y. Zang, H. Zhang, X. Zhang, R. Liu, S. Liu, G. Wang, Y. Zhang and H. Zhao, Fe/Fe_2O_3 nanoparticles anchored on Fe-N-doped carbon nanosheets as bifunctional oxygen electrocatalysts for rechargeable zinc-air batteries, *Nano Res.*, 2016, **9**, 2123–2137.

111 W. Liu, J. Bao, L. Xu, M. Guan, Z. Wang, J. Qiu, Y. Huang, J. Xia, Y. Lei and H. Li, $NiCo_2O_4$ ultrathin nanosheets with oxygen vacancies as bifunctional electrocatalysts for Zn-air battery, *Appl. Surf. Sci.*, 2019, **478**, 552–559.

112 J. Ding, S. Ji, H. Wang, H. Gai, F. Liu, B. Pollet and R. Wang, N-doped porous transition metal-based carbon nanosheet networks as a multifunctional electrocatalyst for rechargeable zinc-air batteries, *Chem. Commun.*, 2019, **55**, 2924–2927.

113 Y. Chen, Y. Guo, H. Cui, Z. Xie, X. Zhang, J. Wei and Z. Zhou, Bifunctional electrocatalysts of MOF-derived Co-N/C on bamboo-like MnO nanowires for high-performance liquid- and solid-state Zn–air batteries, *J. Mater. Chem. A*, 2018, **6**, 9716–9722.

114 T. Zhou, W. Xu, N. Zhang, Z. Du, C. Zhong, W. Yan, H. Ju, W. Chu, H. Jiang, C. Wu and Y. Xie, Ultrathin cobalt oxide layers as electrocatalysts for high-performance flexible Zn–air batteries, *Adv. Mater.*, 2019, **31**, e1807468.

115 S. Li, C. Cheng, X. Zhao, J. Schmidt and A. Thomas, Active salt/silica-templated 2D mesoporous FeCo-N_x-carbon as bifunctional oxygen electrodes for zinc-air batteries, *Angew. Chem., Int. Ed.*, 2018, **57**, 1856–1862.

116 J. Ren, G. Yuan, C. Weng, L. Chen and Z. Yuan, Hierarchically porous heteroatoms-doped Vesica-like carbons as highly efficient bifunctional electrocatalysts for Zn–air batteries, *ChemCatChem*, 2018, **10**, 5297–5305.